Inorganic Chemistry

Article

pubs.acs.org/IC

Role of Cation Interactions in the Reduction Process in Plutonium–Americium Mixed Oxides

Renaud C. Belin,*[,†] Philippe M. Martin,[†] Jacques Lechelle,[†] Muriel Reynaud,[†] and Andreas C. Scheinost[‡]

[†]CEA, DEN, DEC, Cadarache F-13108 Saint-Paul-Lez-Durance, France

[‡]Helmholtz Zentrum Dresden-Rossendorf (HZDR), Institute of Resource Ecology, P.O. Box 510119, 01314 Dresden, Germany, and Rossendorf Beamline at ESRF, BP 220, F-38043 Grenoble, France

ABSTRACT: The oxygen to metal ratio (O/M) is directly related to oxygen potential, which strongly influences the sintering and irradiation performance of nuclear fuels. A better understanding of these two parameters is therefore of major interest. To further ascertain the correlation between O/M ratio and oxygen potential in Am-bearing MOX, several thermodynamic descriptions are being developed. Despite their differences, they all involve the valence of actinide cations (e.g., U, Pu, and Am) as essential parameters. However, as no experimental data on their valence are available, these models rely on assumptions. In the present work, we coupled X-ray diffraction and X-ray absorption spectroscopy to follow the behavior of Pu and Am in three hypo-stoichiometric, U-free $Pu_{1-y}Am_yO_{2-x}$ compounds. We provide for the first time a quantitative determination of Pu and Am valences, demonstrating that plutonium reduction from Pu^{4+} to Pu^{3+} starts only when americium reduction from Am^{4+} to Am^{3+} is completed. This result fills in an important gap in experimental data, thereby improving the thermodynamic description of nuclear fuels. At last, we suggest that the O/M ratio may evolve at room temperature, especially for high Am content, which is of main concern for the fabrication of Am-loaded MOX and their storage prior to irradiation.

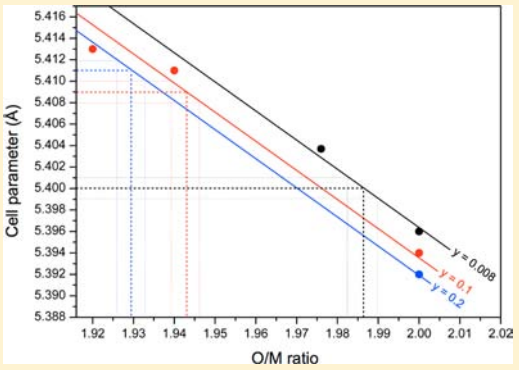

INTRODUCTION

Innovative mixed oxide (MOX) $(U,Pu)O_{2-x}$ fuels for sodium fast neutron reactor (SFRs) systems are currently studied within the framework of the development of fourth generation (GEN-IV) nuclear reactors. SFRs will be able to burn long-lived minor actinides (MA) such as americium. One of the considered options is to add them homogeneously to the fuel in significant amounts (2–6%), imposing new challenges in handling and fabrication due to the higher α and γ activities and the increased neutron release as compared to current uranium oxide fuel. In particular, the decay heat generated by MA fuels already prior to irradiation requires special consideration, such as the use of dedicated fuel handling systems and shipping casks.[1] As a result, decay heat and radiation of minor actinides and fission products (FP) have to be taken into account.

Because the oxygen to metal ratio (O/M) has a direct impact on irradiation performance, a thorough knowledge of its correlation with oxygen potential during manufacturing and storage prior to irradiation is of key interest for the production of fourth generation nuclear fuel.

A study by Osaka et al.[2] highlights a conflicting redox behavior of Am and Pu cations responsible for an unusual oxygen potential versus O/M ratio relationship in Am-bearing MOX. The reason might be (1) the instability of tetravalent Am inherent to the extremely high equilibrium oxygen potential of AmO_{2-x}[3] and (2) the predominance of interactions between U and Am while those between Pu and Am can be neglected.[4] According to these authors and considering the $(U_{1-z-y}Pu_yAm_z)O_{2-x}$ formula, this should result in U being oxidized to a pentavalent state since Am is likely to be trivalent[5] so as to maintain the electrical balance in the oxide for $O/M > 2-z/2$. On the opposite, for $O/M < 2-z/2$, Am should be trivalent and U should remain fully tetravalent, and interactions between Pu and Am become important.

To our knowledge, no experimental data on the valence of actinides and the influence of interactions on their respective local environment are available to assess the reliability of such thermodynamic description. Thus, we recently performed a coupled X-ray diffraction (XRD) and X-ray absorption spectroscopy (XAS) characterization on hypo-stoichiometric Am-bearing MOX $(U_{0.75}Pu_{0.246}\ Am_{0.004})O_{2-x}$.[6,7] We show that Am reduction to Am^{3+} is completed before any reduction of Pu is yet observed, and that no pentavalent U is detectable. Lying in the $O/M < 2-z/2$ region, our results are in agreement with the thermodynamic description of Osaka as the behavior of Am tends to solely influence that of Pu.

For a more thorough insight into the correlated redox behavior of Pu and Am, it is important to study uranium-free hypo-stoichiometric $(Pu,Am)O_{2-x}$ compounds. The knowledge of such interactions is expected to improve the analytical model

Received: October 31, 2012
Published: February 26, 2013

   dx.doi.org/10.1021/ic3023776 | *Inorg. Chem.* 2013, 52, 2966–2972

describing the unusual oxygen potential versus O/M ratio relationship in $(U_{1-z-y}Pu_yAm_z)O_{2-x}$ compounds.

Studies on the $(Pu,Am)O_{2-x}$ system are rare. Miwa et al. studied the phase relationships in PuO_{2-x} containing 9% Am by XRD, ceramography, and differential thermal analysis, with O/M (M = Pu + Am) ranging from 1.90 to 2.00.[8] Osaka et al.[9] measured the oxygen potential on similar samples using thermogravimetric analysis with H_2O/H_2 gas equilibrium and dilute O_2 gas at 1123, 1273, and 1423 K. Recently, oxygen potential measurements were reported for $Pu_{0.5}Am_{0.5}O_{2-x}$ at T = 1333 K using the electromotive force method.[10] The measured oxygen potentials are discussed based on the assumption that the plutonium reduction (Pu^{4+} to Pu^{3+}) starts once that of americium is completed (Am^{4+} to Am^{3+}). This hypothesis is in agreement with the expected behavior of PuO_2 and AmO_2 binaries under reducing conditions. Indeed, the reduction of AmO_2 is much easier than that of PuO_2. Nevertheless, these investigations involve few crystallographic analyses, and to our knowledge, no experimental confirmation of the expected valence relationships of the cations nor information of their local environment in $Pu_{1-y}Am_yO_{2-x}$ compounds is available.

The aim of the present study is to improve our understanding of the reduction of americium and plutonium cations in $(Pu_{1-y}Am_y)O_{2-x}$ for various y = Am/(Pu + Am) ratios and to fill in the gap in experimental data to improve the thermodynamic description of the observed oxygen potentials. By coupling X-ray diffraction and X-ray absorption spectroscopy, we followed the behavior of Pu and Am in three $(Pu,Am)O_{2-x}$ samples with various atomic fractions of Am: $(Pu_{0.992}Am_{0.008})O_{2-x}$, $(Pu_{0.9}Am_{0.1})O_{2-x}$, and $(Pu_{0.8}Am_{0.2})O_{2-x}$ sintered under the same conditions. As demonstrated in a previous work, XRD is the best technique for determining the periodical long-range order whereas XAS is a very complementary tool thanks to its ability to both quantitatively determine oxidation states of each cation (XANES) and outline potential discrepancies in cation local environments (EXAFS).[11]

Finally, to further investigate the role of cation interactions in the reduction process occurring in plutonium−americium mixed oxides, thermodynamic calculations were performed. They allowed determining the temperature range responsible for fixing the O/M ratio, which is of main interest for MA fuels sintering and their storage prior to irradiation.

EXPERIMENTAL SECTION

Synthesis. To handle actinides, we used special tools and a dedicated glovebox (i.e., leaded glass and gloves) to protect ourselves from γ irradiation. Furthermore, due to the low amount of AmO_2 available to carry out this study and the radio-toxicity of ^{241}Am, the syntheses were limited to 10−20 mg of resulting material. Such quantities did not allow pressing green pellets. $(Pu_{0.9}Am_{0.1})O_{2-x}$ and $(Pu_{0.8}Am_{0.2})O_{2-x}$ compositions were prepared via a conventional powder metallurgical route. Syntheses were realized starting from polycrystalline AmO_2 and PuO_2 powders. First, raw materials were calcinated at 1273 K under air for 10 h in order to remove any potential impurities. For the $(Pu_{0.992}Am_{0.008})O_{2-x}$ sample, no AmO_2 powder was used. The minor fraction of Am was calculated from the aging of the ^{241}Pu isotope. The synthesis process consisted of grinding/mixing simultaneously raw material powders in the appropriate ratios in an agate mortar. To counterbalance the lack of pressed pellets, two consecutive thermal treatments under Ar/5%H_2 (1800 K, 24 h) together with an intermediate grinding were carried out in molybdenum crucibles. The furnace was heated and cooled at the rate of 4°/min. The amount of residual H_2O is unknown. Its effect on the oxygen potential will be discussed in the last section.

XRD Data Collection and Structure Refinement. XRD measurements were performed at room temperature on each sample with a Bragg−Brentano Siemens D5000 X-ray diffractometer using a curved quartz monochromator and copper radiation from a conventional tube source (Kα1 radiation, λ = 1.5406 Å). Powder diffraction patterns were obtained by scanning from 25 to 140° 2Θ using 0.02° step intervals. The procedure is thoroughly described in ref 12. Whole powder pattern decomposition was realized according to the Pawley method[13] using DIFFRAC^{plus} TOPAS V4 software.[14] The background was approximated by a Chebyshev polynomial function with eight terms. The scale factor and background parameters only were first refined, and then the cell parameter and fwhm parameters were varied. A modified Thompson−Cox−Hastings pseudo-Voigt profile function (PV TCHZ) was used to refine the shapes of the peaks. The final pattern plots show good agreement between experimental and calculated patterns. The R_p profile and R_{wp} weighted profile were determined and are given in Table 1.

Table 1. XRD Refinements Obtained with the Pawley Method for $(Pu_{1-y}Am_y)O_{2-x}$ Samples

Am/(Am + Pu)	0.008	0.1	0.2
cell parameter (Å)	5.400(1)	5.409(1)	5.411(1)
R_{wp}	15.14	10.64	11.29
R_p	11.28	8.18	8.07
GoF	1.47	1.12	1.48

XAS Measurements and Data Analysis. For each sample, XAS measurements were performed at the Rossendorf Beamline (BM20) located at the European Synchrotron Radiation Facility (ESRF, Grenoble, France). EXAFS samples were prepared by mixing about 1 mg of material with 20 mg of boron nitride. Samples were then pressed into a thin bar to match the dimension of the illuminating X-ray beam while minimizing the amount of sample required. The pellet was then inserted into a hermetic Teflon container and, in addition, into a sealed polyethylene sample holder to provide a double confinement to fulfill safety requirements. Sample holders were mounted in a closed-cycle He cryostat running at 15 K in order to improve the signal-to-noise ratio and to avoid thermal vibration.

For each sample, XAFS spectra were collected at both L_{III} and L_{II} plutonium edges (18 057 and 22 266 eV) and americium L_{III} edge (18 510 eV). Transmission mode was used for collecting plutonium data. Americium XANES spectra were recorded in fluorescence mode using a 13 element Ge solid-state detector. The spectra were corrected for dead time using a measured relationship between the incoming count rate and selected channel analyzer readings for each channel by using the SixPack software package. This procedure ensured that the absorption peak height measured in fluorescence mode matched that measured in transmission mode. Energy calibrations were performed using a Zr foil (17 998 eV) or a Mo foil (20 000 eV) positioned after the second ionization chamber. The ATHENA software[15] was used for normalizing XANES spectra and extracting EXAFS oscillations from the raw absorption data. Linear functions were used for both pre-edge removal and normalization. The post-edge line for XANES spectra was taken using the minimum position between white line and first oscillation (~+25 eV relatively to E_0 position) and +300 eV after the edge. The E_0 values were taken at the first inflection point using the first zero-crossing value of the second derivative. The position of white line maximum was selected with the first zero-crossing of the first derivative. During XANES linear combinations, E_0 positions of standards were not allowed to vary and the sum of the amplitudes of the standards was constrained to equal 1. Experimental XANES data were fitted between −20 and +30 eV compared to the E_0 position. The goodness of the fit is estimated with both R factor and χ^2 values.

Thermodynamic Calculations. Two series of calculations were made using the Calphad method[16,17] with the FUELBASE, which is a database containing the description of the Gibbs energy of all solid,

dx.doi.org/10.1021/ic3023776 | Inorg. Chem. 2013, 52, 2966−2972

liquid, and gas phases of Pu, Am, and O elements as a function of temperature, pressure, and composition.[18] The database was obtained by means of a least-squares method to fit all of the available experimental data (crystallographic, thermodynamic, and phase diagram data). The thermodynamic equilibrium is calculated by minimization of the total Gibbs energy of the system. In the present work, the Thermo-Calc Software was used.[19]

RESULTS AND DISCUSSION

X-ray Diffraction. To discard the effect of Am α-self-irradiation on the cell parameter, XRD measurements were performed immediately after thermal treatment for $(Pu_{0.9}Am_{0.1})O_{2-x}$ and $(Pu_{0.8}Am_{0.2})O_{2-x}$ samples. Considering the minor amount of Am in the $(Pu_{0.992}Am_{0.008})O_{2-x}$ compound, XRD and XAS were performed concurrently on that sample (i.e., four weeks after thermal treatment). All three XRD patterns undoubtedly show crystallized and monophasic compounds characteristic of a $Fm\bar{3}m$ face-centered cubic solid solution (space group 225) regardless of the americium content (see Figure 1). However, diffraction peaks are broader for the $(Pu_{0.992}Am_{0.008})O_{2-x}$ sample. Cell parameters and refinement results are given in Table 1.

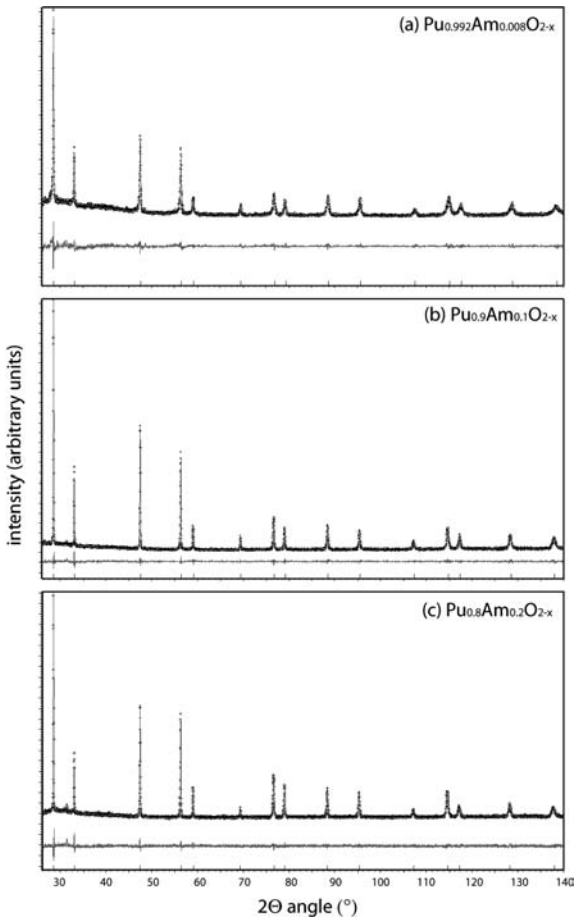

Figure 1. XRD patterns and refinements for $(Pu_{1-y}Am_y)O_{2-x}$ samples.

Figure 2 shows the evolution of the unit cell parameter as a function of the Am/(Am + Pu) ratio for all three samples. The straight line shows the expected cell parameter for a stoichiometric $Pu_{1-y}Am_yO_2$ ideal solid solution obeying Vegard's law based on the admitted cell parameters for PuO_2 and freshly annealed AmO_2.[20,21] Obviously, for all hypo-

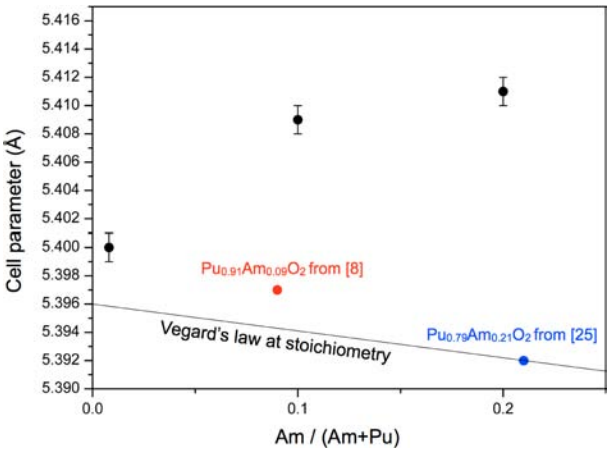

Figure 2. Cell parameter evolution as a function of the Am/(Am + Pu) ratio.

stoichiometric compounds, the relationship between the Am/(Am + Pu) ratio and cell parameter is not straightforward. Cell parameters are much higher and increase nonlinearly with the Am/(Am + Pu) ratio, possibly indicating an enhanced reduction with the Am content.

To better comprehend these results, it is necessary to look further into the crystallographic data available in the literature on the respective binary phase diagrams Pu−O and Am−O and on the Pu−Am−O system. Indeed, few data relative to the hypo-stoichiometric domain are available. Regarding each of the binaries, several studies suggest that PuO_{2-x} is monophasic with a $Fm\bar{3}m$ fluorite structure in a narrow compositional hypo-stoichiometric range. The boundary of this defect phase is still controversial but has been placed at $PuO_{1.98}$.[20,22] Similarly, AmO_2 possesses a narrow monophasic $Fm\bar{3}m$ fluorite domain of existence when $2 > O/M > 1.94$.[21] Below this value, biphasic domains are found. They are composed of the fluorite structure coexisting with a cubic bcc phase (C−Am_2O_3 type) at low temperature and of a bcc phase coexisting with an hexagonal phase at high temperature.[23]

In the Pu−Am−O system, recent studies dealing with the synthesis and the structural characterization of stoichiometric mixed oxides $Pu_{1-y}Am_yO_2$ (y = 0.21; 0.49; 0.80) have been reported.[24] XRD analyses demonstrate that the structure is a cubic solid solution following Vegard's law as evidenced by the cell parameter of the $Pu_{0.79}Am_{0.21}O_2$ compound in Figure 2. Compatibility tests have been realized with $Pu_{1-y}Am_yO_2$ (y = 0.5 or 0.09) and MgO.[25,26] No reaction occurs between mixed oxides and MgO, and two cubic phases (fcc and bcc) are formed.

Considering the mixed valence of both Pu and Am cations, a multiphasic domain similar to that observed in the U−Pu−O system is expected.[27,28] However, for all samples considered in the present work, we only evidenced a monophasic fcc domain. Few studies are available in the hypo-stoichiometric part of the ternary system $Pu_{1-y}Am_yO_{2-x}$ for comparison. Prieur et al. experimentally evidenced a transition from a monophasic fluorite $Pu_{0.80}Am_{0.20}O_{1.98}$ solid solution to a biphasic domain at a temperature lower than 1073 K,[29] and Miwa et al.[8] observed a mixture of two fluorite structures for $Pu_{0.91}Am_{0.09}O_{1.90}$ annealed at 1273 K. They found a single phase fluorite structure for $Pu_{0.91}Am_{0.09}O_{1.94}$ and $Pu_{0.91}Am_{0.09}O_{1.92}$ with cell parameters of 5.411 and 5.413 Å, respectively, and $Pu_{0.91}Am_{0.09}O_{2-x}$ was judged to form a single phase fluorite structure over $0 < x <$

dx.doi.org/10.1021/ic3023776 | Inorg. Chem. 2013, 52, 2966−2972

0.08. However, it is worth noting that the value of 5.397 Å for the cell parameter of the $Pu_{0.91}Am_{0.09}O_2$ stoichiometric compound shows a discrepancy with the expected value of 5.394 Å according to the Vegard's law (see Figure 2). Otobe et al. have observed a single fluorite-type phase over $0.02 < x < 0.22$ for $Am_{0.5}Pu_{0.5}O_{2-x}$.[10]

No systematic variation of cell parameter as a function of oxygen composition has been reported for $Pu_{1-y}Am_yO_{2-x}$. However, based on Haschke et al.[30] and Gardner et al.,[20] a linear evolution is evidenced as illustrated by the black line in Figure 3. Assuming that its slope varies little with y, the Am

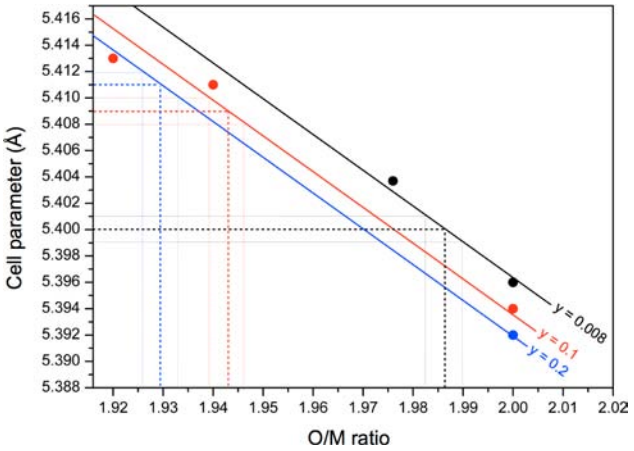

Figure 3. Cell parameter variation as a function of oxygen composition assuming a similar evolution for PuO_{2-x}[30] (black), $Pu_{0.91}Am_{0.09}O_2$[8] (red) and $Pu_{0.79}Am_{0.21}O_2$[24] (blue) - The dotted lines allow estimating the O/M ratio from the cell parameter values for each sample.

content, the red and blue straight lines can be deduced for y = 0.1 and 0.2, respectively. The intercept is the corrected value of 5.394 Å for $Pu_{0.91}Am_{0.09}O_2$[8] and that of 5.392 Å for $Pu_{0.79}Am_{0.21}O_2$.[24] Then, Figure 3 can be used to extrapolate the O/M ratio from the cell parameter of each sample. For $(Pu_{0.992}Am_{0.008})O_{2-x}$, 5.400(1) Å leads to a O/M close to 1.985(5), near the expected boundary of the monophasic domain.[22] For $(Pu_{0.9}Am_{0.1})O_{2-x}$ and $(Pu_{0.8}Am_{0.2})O_{2-x}$ samples, O/M ratios are, respectively, estimated to be 1.945(5) and 1.930(5).

X-ray Absorption Spectroscopy. XANES spectra collected for Pu and Am cations are compared with reference compounds in Figures 4 and 5, respectively. The energy positions of inflection points and white lines are given in Table 2. As the Pu^{4+} reference, we used a spectrum collected on stoichiometric PuO_2 and as the Pu^{3+} reference, a spectrum collected on (U^{4+},Pu^{3+}) mixed oxalate.[31] As an Am^{4+} reference, we used a spectrum collected on stoichiometric AmO_2 and as an Am^{3+} reference, a spectrum collected on a $U_{0.8}Am_{0.2}O_{2-x}$.[32]

Plutonium-L_{III} XANES shows no noticeable variation from the PuO_2 reference compound for both $Pu_{0.9}Am_{0.1}O_{2-x}$ and $Pu_{0.8}Am_{0.2}O_{2-x}$ samples; that is, plutonium remains tetravalent. Regarding the $Pu_{0.992}Am_{0.008}O_{2-x}$ sample, a different behavior is observed with a significant shift of both white line maxima (best viewed in Figure 6) and first inflection point to a lower energy. Thus, a partial reduction of Pu^{4+} to Pu^{3+} is clearly evidenced.

Considering the minor amount of Am present in the $Pu_{0.992}Am_{0.008}O_{2-x}$ sample, americium-L_{III} XANES did not reveal any accurate information regarding Am valence. On the other hand, for both $Pu_{0.9}Am_{0.1}O_{2-x}$ and $Pu_{0.8}Am_{0.2}O_{2-x}$

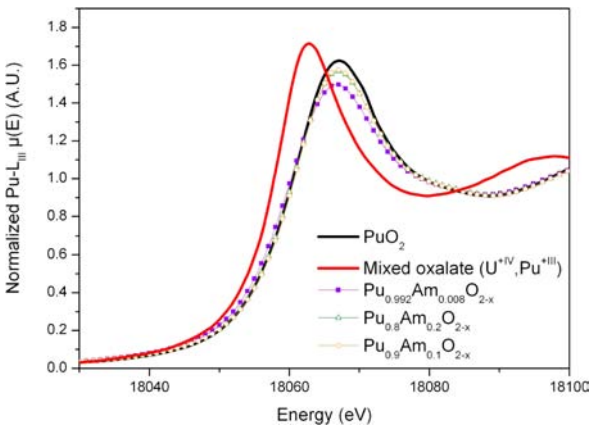

Figure 4. XANES spectra at plutonium-L_{III} edge of our three $(Pu_{1-y}Am_y)O_{2-x}$ samples compared with reference compounds (solid lines).

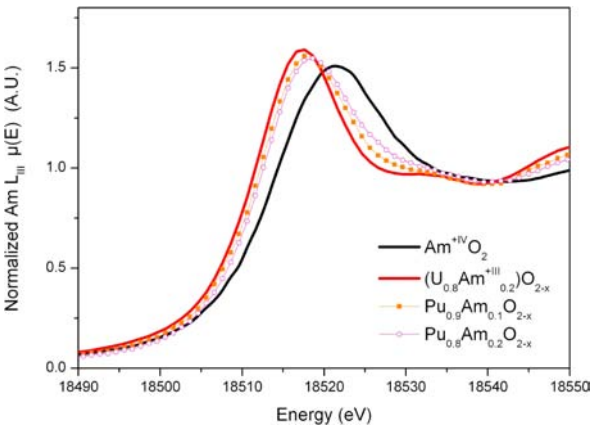

Figure 5. XANES spectra at americium-L_{III} edge of $(Pu_{0.9}Am_{0.1})O_{2-x}$ and $(Pu_{0.8}Am_{0.2})O_{2-x}$ samples compared with reference compounds (solid lines).

Table 2. Position of the Inflection Point and of the White Line of the XANES Spectra

sample	Pu L_{III} edge inflection point (eV)	white line (eV)	Am L_{III} edge inflection point (eV)	white line (eV)
$Pu_{0.992}Am_{0.008}O_{2-x}$	18060.3	18066.8		
$Pu_{0.9}Am_{0.1}O_{2-x}$	18061.2	18067.1	18512.7	18518.2
$Pu_{0.8}Am_{0.2}O_{2-x}$	18061.1	18067.0	18513.2	18518.5
AmO_2[32]			18514.2	18521.5
$(U_{0.80}Am_{0.20})O_{2-x}$			18512.3	18517.7
PuO_2	18061.4	18067.1		
(U^{4+},Pu^{3+}) mixed oxalate[31]	18058.9	18062.8		

samples, both inflection point (E_0) and white line maxima positions are between those of Am^{4+} and Am^{3+} reference compounds, indicating a combination of both valences for Am (see Figure 7). Thus, Am is not totally reduced despite the two consecutive reductive thermal treatments. On the opposite, several XAS studies on the U−Am−O system[32,33] and the $Th_{0.80}Am_{0.20}O_{2-x}$ compound[34] report that Am is totally reduced to the trivalent state after sintering under reducing conditions. There is clearly a different effect of the fluorite matrix PuO_2.

By fitting XANES spectra collected on all three samples with a linear combination of reference compounds, relative

dx.doi.org/10.1021/ic3023776 | Inorg. Chem. 2013, 52, 2966−2972

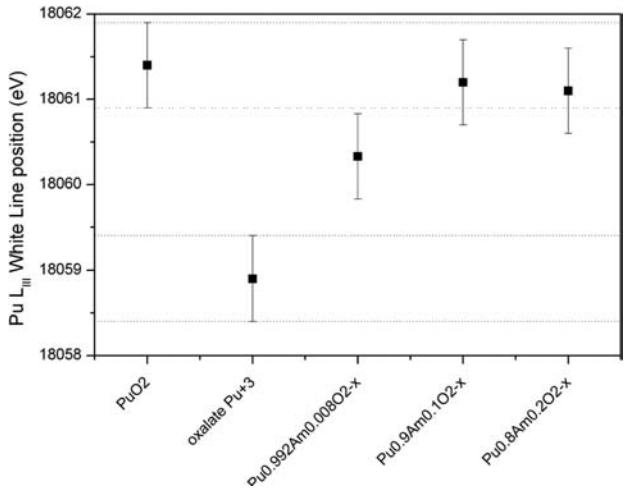

Figure 6. White line maxima position of plutonium-L_{III} edge of $(Pu_{1-y}Am_y)O_{2-x}$ samples compared with reference compounds (solid lines).

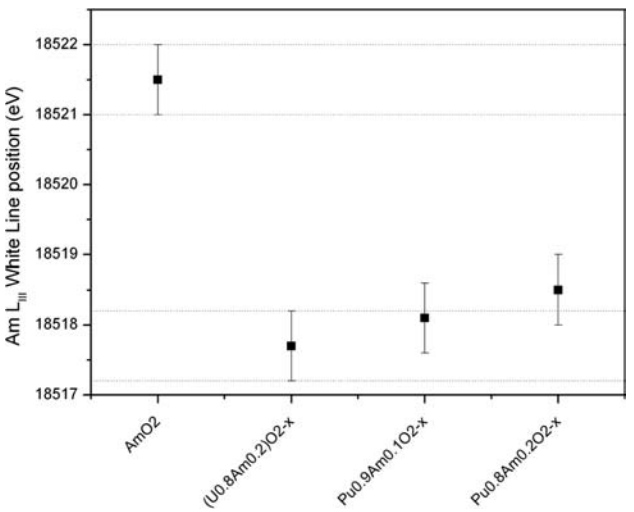

Figure 7. White line maxima position of americium-L_{III} edge of $(Pu_{0.9}Am_{0.1})O_{2-x}$ and $(Pu_{0.8}Am_{0.2})O_{2-x}$ samples compared with reference compounds.

concentrations of Pu^{3+}/Pu^{4+} valences and of Am^{3+}/Am^{4+} valences could be determined. Results are given in Table 3. On the basis of these values, the O/M ratio of each sample was calculated.

For both $Pu_{0.9}Am_{0.1}O_{2-x}$ and $Pu_{0.8}Am_{0.2}O_{2-x}$ samples, the O/M is in good agreement with the value deduced from Figure 3, considering the uncertainties. However, it tends to a slightly higher value, possibly revealing a moderate reoxidation of the material. On the opposite, the O/M value of 1.92(2) is obviously lower than the value of 1.985(5) for $Pu_{0.992}Am_{0.008}O_{2-x}$. As previously mentioned, XRD and XAS were carried out simultaneously only on the latter sample. Over the X-ray spectrum, the penetration depth in a material varies by several orders of magnitude. The copper Kα1 radiation of the laboratory X-ray source has an energy of ~8 keV as compared to the ~18−22 keV energy spectrum used for XAS. For an incident angle of 90°, penetration depths are typically of 1 μm and 10−15 μm with XRD and XAS, respectively.[35] Laser granulometry measurements carried out on the initial stoichiometric $Pu_{0.992}Am_{0.008}O_2$ powder show that it is mostly composed of 10−20 μm particles. Thus, XRD only probes the outer surface, whereas XAS provides information within the whole volume and is more likely to allow determining the true O/M average value. We believe the surface of the particles oxidized at room temperature over the period of a few weeks from the synthesis to XAS experiments. This oxidation might be responsible for this apparent discrepancy in the O/M values determined with both methods. This is also consistent with the broadening of diffraction peaks observed for $Pu_{0.992}Am_{0.008}O_{2-x}$ as compared to $Pu_{0.9}Am_{0.1}O_{2-x}$ and $Pu_{0.8}Am_{0.2}O_{2-x}$, whose XRD patterns were recorded a few days after synthesis.

Osaka et al. have discussed the oxygen partial pressure versus deviation from stoichiometry for $(Pu_{1-y}Am_y)O_{2-x}$ compounds.[9] Their thermodynamic model is based on the statement that Am is reduced first from a tetravalent to a trivalent state, and that after all Am is reduced, Pu is similarly reduced. Depending on y, the atomic fraction of Am, the model suggests two O/M regions with different compositions of metal ions. The first region corresponds to $O/M > 2-y/2$ and is expressed with the following formula: $Pu^{4+}_{1-y}Am^{4+}_{y-w}Am^{3+}_{w}O_{2-w/2}$. The second region corresponds to $O/M < 2-y/2$ and is expressed with $Pu^{4+}_{1-y-v}Pu^{3+}_{v}Am^{3+}_{y}O_{2-y/2-v/2}$.

In this model, valence state changes of Am and Pu in the oxide were only assumed, as no experimental information on such a topic is available. In the present work, we were able to gain such information. Considering $2-y/2$ as the boundary O/M ratio separating both regions, the comparison of our results with Osaka's model is summarized in Table 4.

Table 4. O/M Ratio Calculated from the XANES Analysis Compared to the Boundary O/M and Expected Cation Valence from Osaka's Model[9]

sample	O/M from XAS	boundary O/M	O/M region	expected cations valence
$Pu_{0.992}Am_{0.008}O_{2-x}$	1.92(2)	1.996	second	Pu^{4+} Pu^{3+} Am^{3+}
$Pu_{0.9}Am_{0.1}O_{2-x}$	1.96(2)	1.95	first	Pu^{4+} Am^{3+} Am^{4+}
$Pu_{0.8}Am_{0.2}O_{2-x}$	1.94(2)	1.90	first	Pu^{4+} Am^{4+} Am^{3+}

The $Pu_{0.992}Am_{0.008}O_{2-x}$ composition is obviously located in the second O/M region. XANES analysis reveals a combination of Pu^{3+} and Pu^{4+} valences, which is consistent with Osaka's model. However, due to the low amount of Am in the

Table 3. Plutonium and Americium Cation Repartition (%) and O/M Ratio Calculated from the XANES Analysis Compared to That Extrapolated from Figure 3

	plutonium repartition				americium repartition				O/M	
sample	Pu^{4+}	Pu^{3+}	R factor	χ^2	Am^{4+}	Am^{3+}	R factor	χ^2	XAS	XRD
$Pu_{0.992}Am_{0.008}O_{2-x}$	83(2)	17(2)	8×10^{-4}	0.03					1.92(2)	1.985(5)
$Pu_{0.9}Am_{0.1}O_{2-x}$	98(2)	2(2)	5×10^{-4}	0.02	24(2)	76(2)	8×10^{-5}	0.01	1.96(2)	1.945(5)
$Pu_{0.8}Am_{0.2}O_{2-x}$	98(2)	2(2)	4×10^{-4}	0.02	42(2)	58(2)	6×10^{-4}	0.02	1.94(2)	1.930(5)

dx.doi.org/10.1021/ic3023776 | Inorg. Chem. 2013, 52, 2966−2972

compound, we were not able to experimentally verify the complete reduction of Am^{4+} to Am^{3+}, which the model assumes based on thermogravimetric analyses.

Both the $(Pu_{0.9}Am_{0.1})O_{2-x}$ and the $(Pu_{0.8}Am_{0.2})O_{2-x}$ compositions are found in the first O/M region and involve mostly tetravalent Pu together with a negligible amount of trivalent Pu and a combination of Am^{3+} and Am^{4+} valence. These three results constitute an independent justification of the essential hypothesis inherent to Osaka's model; that is, Am cations will reduce to the trivalent state prior to any reduction of Pu cations.

Thermodynamic Calculations. To further understand the role of actinide valence on sintering, thermodynamic calculations were carried out. As previously mentioned, although several phases within the Pu−Am−O system are likely to occur, only one fcc phase was observed in the present work for all three compositions. Thus, calculations take into account no more than one fcc structure as a solid-state phase with the assumption that it exists at any temperature and does not exhibit any phase separation during cooling.

In a first step, the equilibrium oxygen potential is calculated as a function of temperature using the O/M ratio determined from XAS at 15 K for each sample. Thus, considering the $Pu_{1-y}Am_yO_{2-x}$ composition, the following (y,x) pairs were taken into account: (0.008;0.08), (0.1;0.04), and (0.2;0.06). Since the amount of oxygen impurities in the gas phase was unknown, several values within the range of 2×10^{-5} vpm H_2O through 1000 vpm H_2O have been tested with the result shown Figure 8. The intersection of each $\mu O_2(T)$ curve with the two

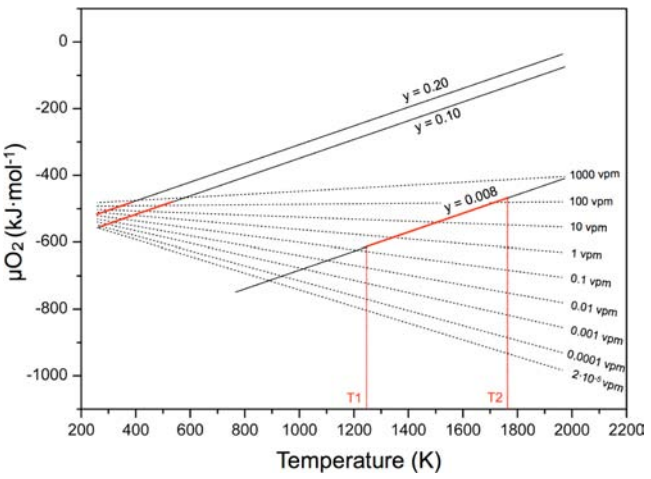

Figure 8. Equilibrium oxygen potential under Ar/5%H_2 of $Pu_{1-y}Am_yO_{2-x}$ for (y,x) = (0.008;0.08), (0.1;0.04), and (0.2;0.06) as a function of temperature taking into account a single fcc solid phase.

extreme H_2/H_2O equilibrium lines gives the range of temperature for which the O/M ratio is likely to be fixed during cooling. It is interesting to note that, regardless of the atmosphere composition, the temperature range is broad and between 900 and 2000 K for the y = 0.008 sample, but it is surprisingly restricted above room temperature for high Am contents (i.e., y = 0.1 and y = 0.2).

In a second step, for each sample, Pu and Am valence states used in the model were compared with Pu^{3+}/Pu^{4+} and Am^{3+}/Am^{4+} repartitions determined from XAS for all H_2/H_2O equilibrium lines. The closest matching values are shown in Table 5 and define an equilibrium oxygen potential domain as well as a more limited temperature range (T_1-T_2) as represented by the red lines in Figure 8.

Table 5. Temperature Range (T_1-T_2) by Comparing Pu^{3+}/Pu^{4+} and Am^{3+}/Am^{4+} Repartitions Obtained from XAS and That Calculated from the Model

	Pu repartition		Am repartition			
sample	Pu^{4+}	Pu^{3+}	Am^{4+}	Am^{3+}	T_1	T_2
$Pu_{0.992}Am_{0.008}O_{2-x}$	85	15			1250	1773
$Pu_{0.9}Am_{0.1}O_{2-x}$	100	0	20	80	293	533
$Pu_{0.8}Am_{0.2}O_{2-x}$	100	0	40	60	273	393

For $Pu_{0.992}Am_{0.008}O_{2-x}$, the O/M ratio may be fixed between 1250 and 1773 K, depending on the oxygen potential within the range of −500 to −610 kJ·mol^{-1}. On the opposite, for both $Pu_{0.9}Am_{0.1}O_{2-x}$ and $Pu_{0.8}Am_{0.2}O_{2-x}$ samples, it is fixed in a narrow range of temperature that comes close to room temperature if the oxygen potential is approximately equal to −550 kJ·mol^{-1}. Indeed, the higher the Am content, the lower the temperature responsible for fixing the O/M ratio.

The decay heat generated during handling and transportation of Am-bearing MOX prior to irradiation leads to an increase in the temperature of the fuel sub-assembly. Actually, to prevent creep damage of the cladding material, it has to be maintained below 650 K.[36] Within room temperature and 650 K, a spontaneous evolution of O/M ratio is likely to occur during storage prior to irradiation as suggested by our calculations. This result is supported by the coupled XRD−XAS analysis demonstrating that the samples have partially oxidized during storage at room temperature with a significant kinetics, that is, within a few weeks after synthesis.

CONCLUSION

The present study provides essential structural data on the Pu−Am−O system as well as quantitative experimental information on Pu and Am valences useful to the comprehension of the overall reduction process occurring in this complex system.

We synthesized hypo-stoichiometric mixed actinide oxides $Pu_{1-y}Am_yO_{2-x}$ (0.008; 0.1; 0.2) by solid-state reaction and performed their structural characterization with XRD and XAS. Thanks to the XANES ability to selectively probe each cation and determine the fraction of ions in a +III or +IV oxidation state, we quantitatively determined Am and Pu valences for each composition and noticed that samples have oxidized during storage.

We compared our results to Osaka et al.'s thermodynamic description and were able to verify its main assumption; that is, when the O/M ratio deviates from stoichiometry, Am is reduced first from a tetravalent to a trivalent state; then after all the Am is reduced, Pu reduction proceeds.

Thermodynamic calculations suggest that, when the Am content increases, the O/M ratio may vary during cooling up to low temperatures. Eventually, depending on the atmosphere, the O/M ratio is still likely to evolve at room temperature. Such a statement is of main concern in the prospect of the fabrication and of the storage prior to irradiation of Am-loaded MOX fuels for fourth generation nuclear reactors.

dx.doi.org/10.1021/ic3023776 | Inorg. Chem. 2013, 52, 2966−2972

AUTHOR INFORMATION

Corresponding Author

*Phone: +33-4-4225-4954. Fax: +33-4-1225-4717. E-mail: renaud.belin@cea.fr.

Notes

The authors declare no competing financial interest.

ACKNOWLEDGMENTS

The MATAV ceramics basic research program of the Nuclear Energy Division at CEA and the F-Bridge Project supported this work.

REFERENCES

(1) *Status of Minor Actinide Fuel Development*; IAEA Nuclear Energy Series: Vienna, 2009.
(2) Osaka, M.; Namekawa, T.; Kurosaki, K.; Yamanaka, S. *J. Nucl. Mater.* **2005**, *344*, 230−234.
(3) Casalta, S.; Matzke, H.; Prunier, C. In *Proceedings of the International Conference GLOBAL95*; Versailles, France, 1995.
(4) Osaka, M.; Kurosaki, K.; Yamanaka, S. *J. Alloys Compd.* **2007**, *428*, 355−361.
(5) Osaka, M.; Sato, I.; Namekawa, T.; Kurosaki, K.; Yamanaka, S. *J. Alloys Compd.* **2005**, *397*, 110−114.
(6) Martin, P. M.; Belin, R. C.; Robisson, A. C.; Dumas, J. C.; Scheinost, A. C. In *Actinide XAS 2011 Conference Hyogo, Japan*; Hyogo, Japan, 2011.
(7) Martin, P. M.; Belin, R. C.; Robisson, A. C.; Scheinost, A. C. In *Plutonium Futures—The Science Keystone*; Keystone, CO, 2010.
(8) Miwa, S.; Osaka, M.; Yoshimochi, H.; Tanaka, K.; Kurosaki, K.; Uno, M.; Yamanaka, S. *J. Alloys Compd.* **2007**, *444−445*, 610−613.
(9) Osaka, M.; Kurosaki, K.; Yamanaka, S. *J. Nucl. Mater.* **2006**, *357*, 69−76.
(10) Otobe, H.; Akabori, M.; Arai, Y. *J. Nucl. Mater.* **2009**, *389*, 68−71.
(11) Belin, R. C.; Martin, P. M.; Valenza, P. J.; Scheinost, A. C. *Inorg. Chem.* **2009**, *48*, 5376−5381.
(12) Belin, R. C.; Valenza, P. J.; Reynaud, M. A.; Raison, P. E. *J. Appl. Crystallogr.* **2004**, *37*, 1034−1037.
(13) Pawley, G. S. *J. Appl. Crystallogr.* **1981**, *14*, 357−361.
(14) *TOPAS V3: General Profile and Structure Analysis Software for Powder Diffraction Data, User'S Manual*; Bruker AXS: Karlsruhe, Germany, 2005.
(15) Ravel, B.; Newville, M. *J. Synchrotron. Radiat.* **2005**, *12*, 537−541.
(16) Lukas, H.; Fries, S. G.; Sundman, B. *Computational Thermodynamics—The Calphad Method*; Cambridge University Press: London, 2007.
(17) Devanathan, R.; Brutzel, L. V.; Chartier, A.; Guéneau, C.; Mattsson, A. E.; Tikare, V.; Bartel, T.; Besmann, T.; Stan, M.; Uffelen, P. V. *Energy Environ. Sci.* **2010**, *3*, 1406−1426.
(18) Gotcu-Freis, P.; Colle, J.-Y.; Guéneau, C.; Dupin, N.; Sundman, B.; Konings, R. J. M. *J. Nucl. Mater.* **2011**, *414*, 408−421.
(19) Sundman, B.; Jansson, B.; Andersson, J. O. *Calphad* **1985**, 153.
(20) Gardner, E. R.; Markin, T. L.; Street, R. S. *J. Inorg. Nucl. Chem.* **1965**, *27*, 541−551.
(21) Chikalla, T. D.; Eyring, L. *J. Inorg. Nucl. Chem.* **1968**, *30*, 133−145.
(22) Chikalla, T. D.; McNeilly, C. E.; Skavdahl, R. E. *J. Nucl. Mater.* **1964**, *12*, 131−41.
(23) Lebreton, F.; Belin, R. C.; Delahaye, T.; Blanchart, P. *J. Solid State Chem.* **2012**, *196*, 217−224.
(24) Jankowiak, A.; Maillard, C.; Donnet, L. *J. Nucl. Mater.* **2009**, *393*, 87−91.
(25) Jankowiak, A.; Jorion, F.; Maillard, C.; Donnet, L. *Nucl. Sci. Eng.* **2008**, *160*, 378−384.
(26) Miwa, S.; Ishi, Y.; Osaka, M. *J. Nucl. Mater.* **2009**, *389*, 402−406.
(27) Guéneau, C.; Dupin, N.; Sundman, B.; Martial, C.; Dumas, J.-C.; Gossé, S.; Chatain, S.; Bruycker, F. D.; Manara, D.; Konings, R. J. M. *J. Nucl. Mater.* **2011**, *419*, 145−167.
(28) Truphémus, T.; Belin, R. C.; Richaud, J.-C.; Reynaud, M.; Martinez, M.-A.; Félines, I.; Arredondo, A.; Miard, A.; Dubois, T.; Adenot, F.; Rogez, J. *J. Nucl. Mater.* **2013**, *432*, 378−387.
(29) Prieur, D.; Carvajal-Nunez, U.; Vitova, T.; Somers, J. *Eur. J. Inorg. Chem.* **2013**, DOI: 10.1002/ejic.201201294.
(30) Haschke, J. M.; Allen, T. H.; Morales, L. A. *Science* **2000**, *287*, 285−287.
(31) Grandjean, S.; Arab-Chapelet, B.; Robisson, A. C.; Abraham, F.; Martin, P.; Dancausse, J.-P.; Herlet, N.; Léorier, C. *J. Nucl. Mater.* **2009**, *385*, 204−207.
(32) Prieur, D.; Martin, P. M.; Jankowiak, A.; Gavilan, E.; Scheinost, A. C.; Herlet, N.; Dehaudt, P.; Blanchart, P. *Inorg. Chem.* **2011**, *50*, 12437−12445.
(33) Nishi, T.; Nakada, M.; Suzuki, C.; Shibata, H.; Okamoto, Y.; Akabori, M.; Hirata, M. *J. Nucl. Mater.* **2011**, *418*, 311−312.
(34) Carvajal-Nunez, U.; Prieur, D.; Vitova, T.; Somers, J. *Inorg. Chem.* **2012**, *51*, 11762−11768.
(35) Henke, B. L.; Gullikson, E. M.; Davis, J. C. *At. Data Nucl. Data Tables* **1993**, *54*, 181−342.
(36) Kato, A.; Chikazawa, Y.; Obata, H. *Nucl. Eng. Des.* **2012**, *247*, 98−105.